Polymerization of 1-Octene by a Pyridylamidohafnium Catalyst: A SEC, ^{1}H NMR and Small Angle Neutron Scattering Study

Aizhen Niu, Jörg Stellbrink, Jürgen Allgaier,* and Dieter Richter

Institut für Festkörperforschung, Forschungszentrum Jülich GmbH, 52425 Jülich, Germany

Rudolf Hartmann

Institut für Biologische Informationsverarbeitung 2, Forschungszentrum Jülich GmbH, 52425 Jülich, Germany

Gregory J. Domski and Geoffrey W. Coates

Department of Chemistry and Chemical Biology, Baker Laboratory, Cornell University, Ithaca, New York 14853-1301

Lewis J. Fetters

School of Chemical and Bimolecular Engineering, Cornell University, Ithaca, New York 14853-5201

Received September 5, 2008; Revised Manuscript Received December 5, 2008

ABSTRACT: We assayed the polymerization of 1-octene in toluene-d_8 polymerized by a pyridylamidohafnium catalyst precursor activated by the cocatalyst tris(pentafluorophenyl)boron. In situ small angle neutron scattering and ^{1}H NMR spectroscopy were used together with time-resolved SEC to investigate the polymerization process. The catalyst system contains several polymerization active species. About 98% of the active catalyst is of uniform activity. The resulting polymers show relatively narrow molecular weight distributions. The residual catalyst exhibits an increased activity, leading to the formation of notably higher molecular weights than is generated by the majority of available active centers. With the help of NMR and SEC results the small angle neutron scattering data could be interpreted quantitatively. Good agreement was found between the expected scattering profile for nonaggregated chains and their measured counterparts. At no stage during the polymerization process could more than single polymer chains be detected.

Introduction

A facet of certain ionic metallocene catalysts is the capacity in olefin polymerizations to undergo self-assembly in hydrocarbons of the resulting propagating head groups.[1−7] Mainly dynamic NMR techniques were used to study the aggregation behavior. In solvents like nonpolar aromatic hydrocarbons or moderately polar chlorinated hydrocarbons the ion aggregates take the generic form of $[LMR^+---X^-]_n$. M denotes Hf, Ti, or Zr, n the average association state (2 or higher), L the ancillary ligand set, and X the weakly coordinating anion. In the catalyst R represents an alkyl group while in the polymerizing state it is the growing polymer chain. In 1999, the first evidence was reported on the formation of the ion quadruples containing zirconocene cations and fluorinated tetraphenyl or methyltriphenylborate anions in benzene.[1] Later reports revealed that aggregate formation depends on catalyst concentration and on solvent identity. The cocatalyst, forming the counterion, is of special importance. Boron compounds like tris(pentafluorophenyl)boron or MAO were examined. Both, the chemical nature of the cocatalyst and its concentration influence aggregation. It was found that the weaker its coordinating abilities are the more aggregate formation can occur.[4,5,7−10] However, it should be pointed out that in all previous cases catalysts, but not polymerizing systems, were investigated. Therefore it is not known to which extent the knowledge gained with the examination of the catalysts can be transferred to polymerization processes. The study of aggregation phenomena is not only interesting from the structural aspect since the aggregation state can significantly influence catalyst activity and polymerization behavior. This was demonstrated using bimetallic catalysts, which can be regarded as models for aggregated systems. Compared to their monometallic analogs significant rate and selectivity differences were found.[11,12]

We have studied headgroup aggregation phenomena taking place during the anionic polymerization of butadiene with *tert*-butyllithium in aliphatic hydrocarbon solvents.[13−15] A combination of small angle neutron scattering (SANS) and ^{1}H NMR was used in that case. SANS is the ideal tool to structurally investigate polymer systems. Its spatial resolution ranges from 5 to 1000 Å and covers the size range from oligomers to aggregated larger polymer chains. If the polymerization reaction is carried out in the neutron beam, time-resolved information is available. In situ ^{1}H NMR yields the time dependent monomer conversion. In the absence of termination reactions the comparison of the signal intensities related to the growing polymer chains and the initiating units allows the calculation of molecular weights of the individual chains. The combination of the single chain information obtained from NMR with the overall structural information from SANS makes it possible to distinguish between aggregated and nonaggregated polymer chains through the duration of the polymerization.

In this work a pyridylamidohafnium catalyst precursor was used. Its chemical structure is shown in Figure 1. Together with the cocatalyst tris(pentafluorophenyl)boron ($B(C_6F_5)_3$ the livingness of the polymerization was demonstrated.[16] This facilitates the examination of potential aggregation phenomena. The catalyst used in this work polymerized propylene having a narrow molecular weight distribution with 56% isotactic content [m^4],[16] which is lower than but comparable to the stereoselec-

* Corresponding author.

10.1021/ma8020294 CCC: $40.75
Published on Web 01/22/2009

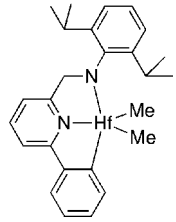

Figure 1. Chemical structure of the pyridylamidohafnium catalyst precursor.

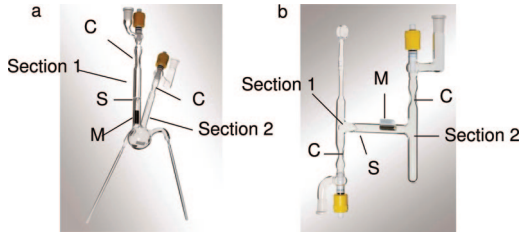

Figure 2. Reactors for the preparation of the NMR (a) and SANS samples (b).

tivity found for other pyridylamidohafnium catalysts.[17−19] In our study the polymerization of 1-octene was studied by in situ SANS and ^{1}H NMR spectroscopy. Furthermore, samples were taken from an additional polymerization experiment at different times for SEC analysis. This allowed the monitoring of molecular weights and molecular weight distributions at different polymerization states.

Experimental Section

All manipulations were carried out on a high vacuum line using standard Schlenk techniques or in a glovebox, filled with argon (M Braun, Unilab). The water level in the glovebox was below 1 ppm and the oxygen level below 0.1 ppm. The flasks for all manipulations were equipped with Teflon stopcocks that allowed the transfer of materials between the vacuum line and glovebox without air contamination. The syringes, pipettes, and vials used for sample preparation were heated on the vacuum line overnight at 150 °C. Small catalyst precursor and cocatalyst quantities could be precisely handled using a Stroehlein ST 220 analytical balance inside the glovebox. Toluene (Merck, ≥99.9%) was degassed, distilled into another flask which contained sodium metal and then stirred for at least 24 h before being degassed again and heated to 110−115 °C for 3−4 h. 1-Octene (98%, Aldrich) and toluene-d_8 (99% D, Chemotrade) were treated in the same way, except that drying was carried out over 3Å molecular sieves. The sieves were activated by heating under high vacuum to 170 °C overnight. Tris(pentafluorophenyl)boron ($B(C_6F_5)_3$), 98%, Strem Chemicals) was degassed under high vacuum for 2 h. The pyridylamidohafnium catalyst precursor was synthesized according to ref 16.

Polymerization Reaction for Time-Resolved SEC Analysis. A 17.7 mg (34.6 μmol) sample of $B(C_6F_5)_3$ was dissolved in 2.7 g of toluene. Then 17.0 mg (30.9 μmol) of catalyst precursor and 0.47 g of 1-octene were dissolved in 2.8 g of toluene in a separate vial. Both solutions were cooled to −8 °C in a freezer, mixed, and immediately split up into five samples using a precooled pipet and vials. The samples were stored at −8 °C and quenched with MeOH after different reaction times. Volatile compounds were removed by pumping under high vacuum overnight. Monomer conversions were calculated from the weights before and after drying taking into consideration the calculated contributions of nonvolatile catalyst precursor and cocatalyst. The dry samples were used without further purification for SEC analysis.

^{1}H NMR Sample Preparation. The reactor for NMR sample preparation is shown in Figure 2a. It consists of two sections separated by break-seal S. Both sections contain Teflon stopcocks, which allowed flame drying of the glassware at the high vacuum line and transfer without air contact to the glovebox. 3.7 mg (6.7 μmol) of catalyst precursor and 0.10 g of 1-octene were dissolved in 1.3 g of toluene-d_8 and filled inside the glovebox into the flask of section 1. 3.0 mg (5.9 μmol) $B(C_6F_5)_3$ dissolved in 1.2 g of toluene-d_8 were filled into section 2. At the vacuum line both sections were cooled to liquid nitrogen temperature. The inert gas was pumped off and the stopcocks were removed by sealing off the glassware at constrictions C. After warming the whole apparatus to −80 °C in a dry ice bath, the toluene solutions were mixed by opening break-seal S with magnet M, located inside the apparatus. Immediately after the mixing procedure the NMR tubes were filled and sealed off. They were kept at liquid nitrogen temperature until the NMR experiment was started.

SANS Sample Preparation. A slightly modified strategy was employed for the SANS samples because the quartz cells tended to break at liquid nitrogen temperature. Therefore the glassware shown in Figure 2b was used. Again the two sections are equipped with Teflon stopcocks and are separated by break-seal S. The sample preparation was similar to the NMR samples. Section 1 was filled with a mixture containing 5.7 mg (10.3 μmol) of catalyst precursor and 0.16 g of 1-octene and 1.6 g of toluene-d_8. Section 2 contained 4.6 mg (9.0 μmol) $B(C_6F_5)_3$ and 2.2 g of toluene-d_8. After sealing off the apparatus at constrictions C it was kept at room temperature. Before the SANS measurement was started break-seal S was opened, the liquids were mixed and transferred into the SANS cell. This way of sample preparation could not be used for the NMR experiments because the NMR setup did not allow a complex apparatus being attached to the NMR tube. In addition the presence of magnetic material near the instrument would have been highly disadvantageous.

SEC Measurements. The SEC experiments were carried out using a PL-GPC 50 instrument. In some cases three Polymer Laboratories PolyPore columns at 30 °C were used (column set 1). For the signal detection a Viscotek Model TDA 300 detector with a differential refractometer (RI) and a right angle laser light scattering (LS) detector were used at 30 °C. The solvent was THF at a flow rate of 1 mL/min, which was degassed using a Viscotek Model VE 7510 instrument. Molecular weights were calculated using the Polymer Laboratories Cirrus GPC software. For the other SEC experiments the same setup was used except that four Polymer Laboratories PLgel 10 μm MIXED-B columns were used (column set 2). The SEC calibration involved 11 polystyrene (PS) standards ranging in molecular weight from 0.50 to 3000 kg/mol. The poly(1-octene) samples had their molecular weights and polydispersity parameters evaluated via the two SEC column sets described, without corrections or adjustments. The validity of this approach was verified by the use of two narrowly distributed poly(1-octene) fractions whose molecular weights (73 and 145 kg/mol) were jointly measured using the polystyrene calibration and online LS. Within the error limits (5−10%) of the two disparate measurement techniques the molecular weight moments (M_n, M_w, and M_z) agreed. Similar behavior was seen for PS standards treated as unknowns. Thus, the PS calibrants can be used for poly(1-octene) characterization. LS detection could not be used for the molecular weight detection of the poly(1-octene) samples investigated in this work (molecular weights smaller than 25 kg/mol). This was caused by the low signal intensities encountered.

^{1}H NMR Experiments. One-dimensional ^{1}H NMR spectra were recorded on a 14.1 T Varian Unity Inova 600 spectrometer at −10 and +20 °C with a standard one pulse experiment and a pulse duration of 7.3 μs. The spectra were acquired with a sweep width of 8000 Hz and 16000 complex data points. For each free induction decay (FID) 4 scans were collected with an acquisition time of 1 s and a 30 s recycling delay between each scan for complete relaxation of the 1% ^{1}H of the toluene-d_8. Processing of the FIDs was done with the MestReC software package. After zerofilling to 32768 complex data points the data were Fourier-transformed. Additional baseline corrections were performed using polynomial functions of the MestRec software. The integral peak intensity is proportional to the number of protons contributing to a signal only if the spin system completely relaxes between consecutive scans.

The experimental quantity observed in a ^{1}H NMR experiment is the peak integral. Since the NMR samples were sealed off, the amount of solvent is constant during the polymerization. One peak of toluene located at 7.21 ppm was used as reference to normalize all the integrals of each spectrum.

SANS Measurements. The SANS measurements were performed at the instruments KWS1 and KWS2 at the Forschungszentrum, Jülich, Germany. We used sample-to-detector distances, D, of 20, 8, 4, 2, and 1.25 m, and collimation lengths, L, of 20, 14, 8, 4, and 2 m, using a neutron wavelength $\lambda = 7.3$ Å with wavelength spreads $\Delta\lambda/\lambda = 20\%$ and 10%, respectively. This covers a Q-range of $2 \times 10^{-3} \leq Q \leq 0.23$ Å^{-1}, which corresponds to a spatial resolution 5 Å $\leq D = 1/Q \leq 500$ Å. The experimental quantity observed in a SANS experiment is the intensity in terms of the macroscopic cross section ($d\Sigma/d\Omega$) as a function of the scattering vector $Q = [4\pi/\lambda](\sin\theta)/2$, with λ the neutron wavelength and Θ the scattering angle. Q has the dimensions of a reciprocal length and can therefore be regarded as an "inverse meter stick".

$$\frac{d\Sigma}{d\Omega}(Q) = \frac{\Delta\rho^2}{N_a} \cdot \phi \cdot V_w \cdot P(Q) \quad (1)$$

Here, ϕ is the volume fraction, V_w the corresponding weight average molecular volume, and $P(Q)$ the form factor of the scattering particles, which contains all structural information. $\Delta\rho$ is the scattering contrast given by

$$\Delta\rho = \rho_0 - \rho = \left[\frac{\Sigma b_0}{v_0} - \frac{\Sigma b_{mon}}{v_{mon}}\right] \quad (2)$$

The ratio $\rho_0 = \Sigma b_0/v_0$ is the scattering length density of the solvent with b_0 the scattering length of the atoms forming the solvent molecule and v_0 the corresponding volume. $\rho = \Sigma b_{mon}/v_{mon}$ is the corresponding quantity for the repeat unit of the scattering particle and N_a the Avogadro number. Since all b_i terms are well defined and tabulated properties of the corresponding nucleus the SANS data are obtained on an absolute scale and can be unambiguously interpreted. For the polymerizing systems we assume the nonreacted octene to be one component of a binary solvent mixture 1-octene/toluene-*d*. Thus we obtain a time-dependent change in contrast factor $\Delta\rho^2(t)/N_A$ of about 6.7% during the polymerization. This is quantitatively taken into account during further data analysis.

In general, all azimuthally averaged data were corrected for empty cell scattering and then normalized to the absolute scattering cross section [cm^{-1}], using a 1.5 mm plexiglass standard. Contributions due to incoherent background and solvent scattering were subtracted from all data sets before analysis. A useful presentation of the theory and practice of SANS for polymeric systems is available from Higgins and Benoit.[20]

Results and Discussion

In our investigation 1-octene was chosen as the monomer since poly(1-octene) is soluble in toluene in the temperature range under investigation (−10 and +20 °C) irrespective of tacticity. The polymerization reactions carried out in the NMR and SANS instruments were performed in flame sealed cells since the catalyst system is highly sensitive to contamination with oxygen or water and the catalyst quantities for the experiments ranged from only 3−10 μmol. Because of the special requirements for the different analysis methods all samples were prepared individually. In Table 1, the polymerization conditions are summarized for the SANS, NMR and SEC experiments. It contains also the final molecular weights, assuming full activity of the catalyst and the absence of termination reactions. The SANS and one NMR experiment were carried out at 20 °C, the other NMR experiment and the polymerizations for SEC sample preparation were accomplished at −10 and −8 °C. For the SEC investigation the temperature of −8 °C was chosen to slow the polymerization reaction in order to obtain samples at low monomer conversion.

Table 1. Polymerization Conditions for the SEC, NMR, and SANS Samples

samples	temperature (°C)	monomer weight fraction (%)	$C_{cat.}$ (mM)	$C_{cat.}/C_{cocat.}$	$M_{n,cal.}$ (kg/mol)
SEC	−8	4.4	3.1	0.9	15.2
NMR	−10	4.0	2.9	1.1	14.9
	20	4.0	2.9	1.1	14.9
SANS	20	4.2	2.9	1.1	15.2

According to ref 16, the ideal conditions for a living polymerization behavior require room temperature, a monomer concentration of approximately 20 vol % and a low concentration of the catalyst system to obtain molecular weights in the order of 100 kg/mol. However, to perform time-resolved measurements the polymerization temperature had to be lowered in some experiments of this work. In addition, for the scattering experiments it was necessary to adapt the molecular weight to the accessible SANS Q-range and to keep the final polymer concentration below the overlap concentration c^*. Therefore a final molecular weight of 15 kg/mol and a final polymer concentration of less than 10 vol % was targeted.

Time Resolved SEC Analysis of the Polymerization Reaction. Under the assumption that each catalyst molecule initiates the growth of one polymer chain, the final polymer M_n, calculated from the amounts of monomer and catalyst was 15.2 kg/mol in this experiment. Samples were taken at different reaction times and analyzed by SEC using column set 1 (see Experimental Section). Figure 3 shows some of the SEC chromatograms using RI-detection. The chromatograms are normalized to the absolute polymer concentration in the polymerization reactor on the basis of the known monomer conversions. The molecular weight characterization results using PS calibration are collected in Table 2 for all samples. The monomer conversions were calculated from the amounts of original sample and after drying. The chromatogram obtained from the earliest sample, taken after 6.7 min. shows a peak having a maximum at an elution time of about 21 min corresponding to 6.54 kg/mol, indicated as P1. In the later chromatograms this signal moves to shorter elution times or higher molecular weights. All signals for P1 show a low molecular weight tailing. It is most prominent for the earliest sample, which explains the larger value for M_w/M_n obtained for this sample. The tailing event is not due to terminated polymer chains since the peak moves to higher molecular weights with reaction time. We assume that the tailing results from a retarded initiation process. This assumption is also supported by the overproportional growth of the P1 signal intensity with time. Under the assumption that the molar amount of polymer forming P1 is constant one would expect that in the normalized chromatograms the signal intensity increases linearly with molecular weight. However the intensity increase from the first

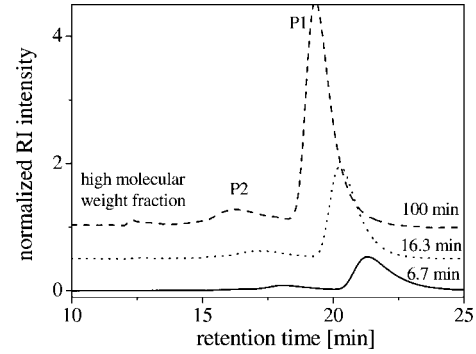

Figure 3. SEC results using RI detection and column set 1 of samples taken at different reaction times.

Table 2. SEC Analysis Results of Samples Taken at Different Reaction Times

reaction time (min)	monomer conversion (%)	P1		P2		catalyst activity (%)
		M_n(kg/mol)	M_w/M_n	M_n (kg/mol)	M_w/M_n	
6.67	16.9	6.54	1.19	48.1	1.28	34
16.3	38.5	12.7	1.12	86.7	1.27	40
39.9	64.7	18.3	1.11	108	1.28	48
62.0	83.1	19.7	1.12	116	1.29	56
100	92.6	22.3	1.12	124	1.23	56

to the last chromatogram is about 50% larger than expected. This can only be explained if the amount of active catalyst forming P1 fraction increased equivalently.

Accompanying the P1 component additional small signals of higher molecular weight are visible. The molecular weights of P2 are considerably higher than those of P1. Their molecular weight distributions are slightly broader. P2 also moves to higher molecular weights with time. The M_n ratio of P2 to P1 is about 7.3 for the first sample and decreases to about 5.6 for the last sample. In agreement with the findings for P1 the catalyst amount forming P2 increases from the first to the last sample by about 50%.

It should be pointed out that signal P2 does not originate from only one polymerization process, although it has a fairly narrow molecular weight distribution. Some of the chromatograms taken from the fully polymerized SANS and NMR samples showed that P2 is composed of different fractions. However, the limits of the resolution power of the SEC columns make it almost impossible to separate the individual signals.

The RI trace of the final sample taken at 100 min shows a third peak at an elution time of about 12.5 min. This signal is hardly visible in the earlier chromatograms. In order to analyze the high molecular weight regions it is helpful to use LS detection. Those results are shown in Figure 4 for the same SEC samples as Figure 3. The chromatograms are normalized in the same way as in Figure 3. In the LS traces the high molecular weight region is highlighted since LS signal intensity is proportional to mass concentration times molecular weight, whereas RI signal intensity is only proportional to mass concentration. It is clearly visible that besides P1 and P2 higher molecular weight material is present in the first sample. The signals at 13.6 min do not move to higher molecular weights with the ongoing polymerization, but intensity increases. The signals at 12.2 min correspond to the upper exclusion volume of column set 1. Therefore these signals represent the sample fractions having higher molecular weights than the upper resolution limit of the columns.

This interpretation was confirmed by additional experiments using the SEC column set capable of resolving the high molecular weight regions of the samples (column set 2, see Experimental Section). RI and LS traces of the final sample at 100 min obtained with this column set are shown in Figure 5. The RI trace resembles the one recorded with column set 1 (Figure 3) except that in the high molecular weight region of the chromatogram no signal is detectable. The LS traces also resemble in the low molecular weight regions. The different signal-to-noise ratios most likely rely on the use of an additional filter in the detector used in combination with column setup 2. In the high molecular weight regions however the LS traces are significantly different. The relatively sharp signals at 13.6 min and at 12.2 min obtained with setup 1 are replaced by one broad high molecular weight signal in the measurement with setup 2. This is a result of the different upper resolution limits. For column set 2 it is about one-half to 1 order of magnitude larger. This is sufficient to resolve the high molecular weight component. The highest molecular weights detectable in the LS traces were estimated on the basis of the PS calibration curve. They range from 5000 kg/mol for the early samples up to 12000 kg/mol for the final sample. However it should be pointed out that the high molecular weight fraction in all cases corresponds to less than 1% of the overall material. Unfortunately, LS detection could not be used in this work for molecular weight evaluation. For the low molecular weight signals the LS intensities and for the high molecular weight signals RI intensities were too low to obtain reliable molecular weights.

The analysis of the RI chromatograms reveals that the mass fraction of P1 increases from 83% in the first sample to 87% in the last sample, whereas P2 decreases from 16% to 11%. The amount of high molecular weight fraction stays approximately constant at less than 1%. From the catalyst viewpoint the scenario is considerably different. Because of the higher molecular weights of the polymer chains represented by P2 it seems that about 2% of the active catalyst is responsible for the production of P2. The catalyst fraction polymerizing the high molecular weight material cannot be quantified precisely, but it stands to reason that it is small.

With the knowledge of monomer conversions and polymer molecular weights the fraction of active catalyst can be calculated for each sample. The values summarized in Table 2 comprise both catalyst fractions forming P1 and P2. For the first sample at a monomer conversion of 16.9% only 34% of the catalyst has already initiated the growth of polymer chains. In agreement with the results mentioned before for P1 and P2 the activity increases to 56% between 64.7% and 83.1% of monomer conversion from where it stays constant until the

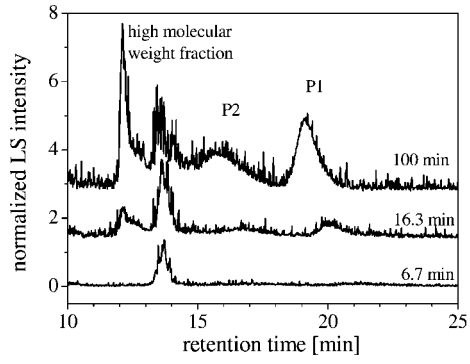

Figure 4. SEC results using LS detection and column set 1 of samples taken at different reaction times.

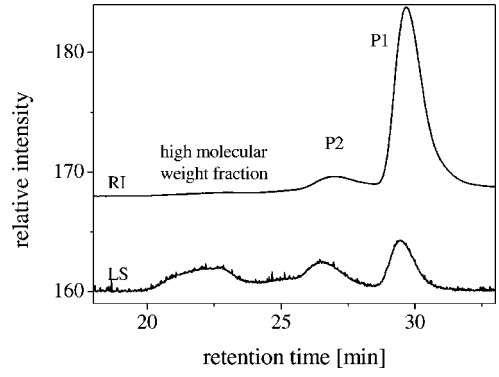

Figure 5. SEC results using RI and LS detection and column set 2 of the final sample at 100 min reaction time.

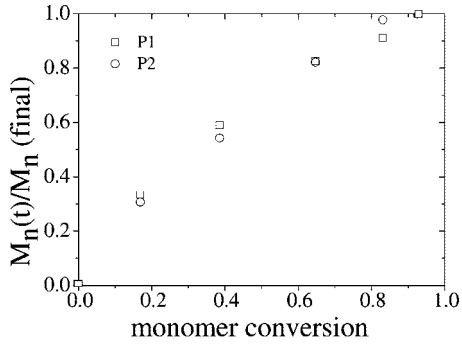

Figure 6. M_n of P1 and P2 normalized to the final M_n values as a function of monomer conversion.

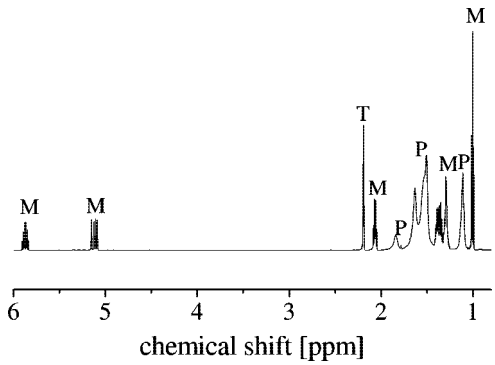

Figure 7. ^{1}H NMR spectrum of the polymerization of 1-octene at −10 °C in toluene-d_8, taken at a reaction time of 72.3 min. Monomer and polymer signals are indicated with M and P respectively while T stands for toluene.

cessation of polymerization. The slow and incomplete initiation originates from the low reaction temperature[16] and low monomer concentration. Under these conditions catalyst decomposition significantly competes with the initiation process. The decomposition reaction is based on an exchange of a C_6F_5 cocatalyst group with a methyl group on Hf.[21]

The increase of the normalized M_n of P1 and P2 with monomer conversion is plotted in Figure 6. It is interesting that for both processes the behavior is almost identical. The nonlinear increase of M_n at low monomer conversions reflects the retarded initiation processes. The slow initiation reactions also contribute strongly to the molecular weight distributions of signals P1 and P2, which are visibly broader than expected for this controlled polymerization. Without this effect one would expect visibly narrower distributions.

Polymerization Kinetics. Time dependent monomer consumption was monitored by ^{1}H NMR at −10 °C and at 20 °C. For these experiments the polymerizations were carried out directly in sealed NMR tubes in the spectrometer. Figure 7 shows a typical NMR polymerization spectrum at −10 °C. The decrease of the vinyl proton signals between 5 and 6 ppm was used as a measure for the monomer concentration. In order to compare different spectra, intensities were normalized to the aromatic toluene signals at 7.2 ppm. In the case of the polymerization at −10 °C, the reaction was slow enough that in the first spectrum almost no polymer was found. The scenario was different at 20 °C. From the initial polymerization stage a large amount of polymer was present. Therefore the original monomer concentration was calculated from the polymer methyl signal intensity at 1.1 ppm of the final sample at full monomer conversion. Figure 8 shows the results obtained from the NMR investigation. In addition the results at −8 °C are presented. Those values result from the samples used for the SEC investigation and were calculated from the sample weights after

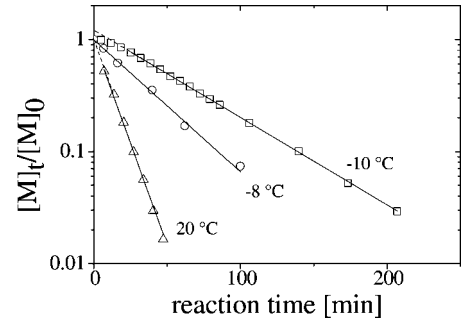

Figure 8. Monomer concentration $[M]_t$ normalized to the initial monomer concentration $[M]_0$ logarithmically plotted against reaction time. The concentrations at −10 and +20 °C were calculated from in situ ^{1}H NMR measurements; the concentrations at −8 °C were calculated from the weights of individually polymerized and dried samples used for the SEC experiments.

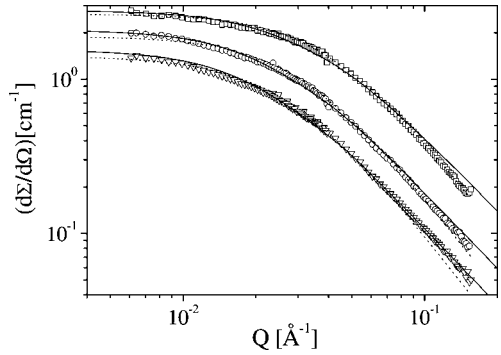

Figure 9. SANS intensity vs scattering vector Q for the terminated polymer at $T = 20$ °C: (▽) 0.99%; (○) 1.77%; (□) 4.34%. Solid lines: fit to the Beaucage form factor. Dotted lines: predictions from SEC (see text).

evaporation of all volatile compounds. For all measurements the logarithm of the normalized monomer concentrations $[M]_t/[M]_0$ drop linearly with time, showing the expected first order reaction kinetics. Only for the reaction at −10 °C is there a deviation for the first 30 min, which reflects the increasing concentration of active catalyst during that period. This behavior is not visible at −8 °C and at 20 °C. At −8 °C most likely the reduced accuracy of the experimental method used in this experiment does not allow the detection of the retarded initiation process. At 20 °C the polymerization is so fast that the first data point corresponds to a monomer consumption of almost 50%.

Time Resolved SANS Analysis. Figure 9 shows SANS intensities in absolute units [cm^{-1}] as a function of scattering vector Q for the terminated polymer. The highest concentration in terms of volume fraction ϕ shown in Figure 9 is the same as that of the polymerizing solution at full monomer conversion. All data can reasonably be described for all Q-vectors using the Beaucage form factor combined with a virial expansion. In detail we fitted all concentrations simultaneously to eq 3 with individual radii of gyration in the Beaucage form factor[22] $P(Q)$:

$$\left(\frac{d\Sigma}{d\Omega}\right)(Q) = \frac{\Delta\rho^2}{N_a}\frac{\phi}{\left[\frac{1}{V_w P(Q)} + 2A_2\phi\right]} \tag{3}$$

This analysis gives an average molecular weight, $M_w = 40700$ g/mol, a radius of gyration extrapolated to zero concentration, $R_{g0} = 97 \pm 2$ Å and a second virial coefficient, $A_2 = 9.23 \times 10^{-4}$ cm^3 mol g^{-2}. During the fitting procedure we fixed the asymptotic slope of the power law $I(Q) \sim Q^{-1/\nu}$ in the high-Q region, $Q \geq 0.08$ Å^{-1}, to the expected value for the Flory

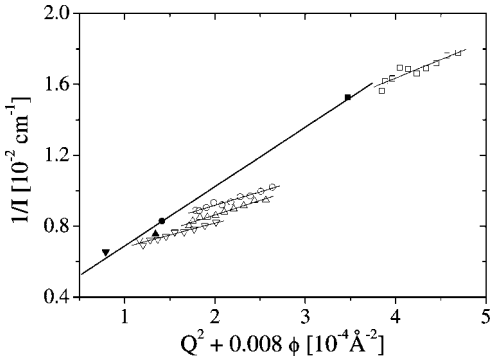

Figure 10. Zimm plot of the terminated polymer: (▽) 0.99%; (Δ) 1.68%; (○) 1.77%; (□) 4.34%.

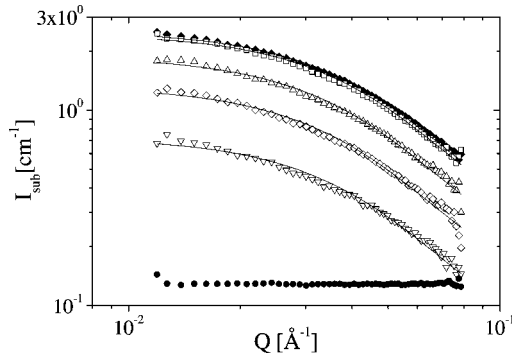

Figure 11. Time dependent SANS intensities vs scattering vector Q during polymerization of 1-octene at 20 °C: (●) monomer, $\phi = 4.13\%$; (▽) 4 min; (◇) 7 min; (Δ) 11 min; (□) 28 min; (◆) terminated polymer. Solid lines: fit to Beaucage form factor.

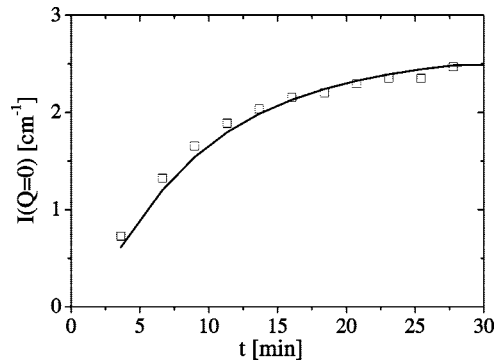

Figure 12. SANS intensity $I(Q=0)$ vs reaction time. Solid line: Expected total SANS intensity from time-resolved SEC (see text).

exponent of a swollen chain ($\nu = 3/5$). Whereas the lowest concentration, $\phi = 0.99\%$, shows a good agreement in the high-Q region, for the highest concentration, $\phi = 4.34\%$, there are some systematic deviations visible. Using $1/\nu$ as free parameter we obtain values of $1/\nu = 1.74 \pm 0.3$ corresponding to $\nu = 0.57$. This value demonstrates that toluene is a good solvent for partially isotactic poly(1-octene).

To cross-check these results a model independent Zimm analysis in the low-Q regime was performed for the terminated polymer (see Figure 10). Also the Zimm analysis gives similar results with respect to molecular weight, $M_w = 43500$ g/mol and second virial coefficient, $A_2 = 9.67 \times 10^{-4}$ cm^3 mol g^{-2}, and only slightly smaller values for the radius of gyration $R_{g0} = 89 \pm 6$ Å.

But our SANS experiments cannot separate the scattering contributions of the individual components of the molecular weight distribution; so we only obtain an average molecular weight, $\overline{M_w}$, an average radius of gyration, $\overline{R_g}$, and an average second virial coefficient, $\overline{A_2}$, if we perform a "stand-alone" analysis. More meaningful is a direct comparison of our experimental SANS data with the expected scattering intensity calculated on basis of our SEC results. This takes into account the polydispersity of the sample (see discussion of the SEC data). The total SANS intensity was calculated assuming a trimodal distribution, i. e. $I_{tot} = I_1 + I_2 + I_3$. I_1, I_2, and I_3 correspond to the scattering contributions of P1, P2, and the high molecular weight fraction. The intensities of the individual components I_i were calculated according to eq 1, using the total polymer volume fraction in the term of the virial coefficient. This is necessary to consider particle interactions between the different components. The values for the individual $R_{g,i}$ were calculated by $R_{g,i} = 0.138\, M_{w,i}^{0.58}$ following ref 23. The resulting curves are also shown in Figure 9 and are in good agreement with the experimental data.

In the next step the polymerization process was examined. Figure 11 shows the time-dependent scattering curves $I(Q)$ vs Q in absolute units [cm^{-1}] obtained by in situ SANS experiments. At 20 °C the polymerization is finished within 30 min, but nevertheless it was possible to obtain SANS data with good counting statistics. The forward scattering $I(Q=0)$ increases with time, reflecting the growth of the polymer chain, but the Q-dependence seems to be constant at all reaction times. Such behavior would indicate a constant characteristic size or length during all stages of the polymerization. For each reaction time the data can be fitted by a Beaucage form factor as in case of the terminated polymer, but now with arbitrary forward scattering amplitude $I(Q=0,t)$. The time-dependence of the amplitude is shown in Figure 12. The continuous increase of the forward scattering $I(Q=0,t)$ can be described by $I(Q=0,t) = I(Q=0,t=\infty)\,(1 - \exp^{-t/\tau})$ with a characteristic time $\tau = 8.3$ min.

To quantify all effects in the polymerizing solution we have to focus on the different time-dependent quantities: The volume fraction of the reacted monomer/formed polymer $\phi(t)$, the molecular weight of the growing chain $M_w(t)$ and its corresponding radius of gyration $R_g(t)$. We have to emphasize once again, that in the polymerizing solution the growing chain with molecular weight $M_w(t)$ is at a finite concentration $\phi(t)$, therefore we measure a concentration dependent apparent $R_g(t,\phi)$.

Let us first discuss the time-dependence of the forward scattering intensity $I(Q=0,t)$, since its derivation is straightforward. According to eq 3 it is given by

$$\left(\frac{d\Sigma}{d\Omega}\right)(Q=0,t) = \frac{\Delta\rho^2}{N_a}\frac{\phi(t)}{\left[\frac{1}{V_w(t)} + 2A_2\phi(t)\right]} \qquad (4)$$

From NMR experiments we know the remaining amount of monomer $\phi_m(t)$ as a function of reaction time t by following the relative decrease of the monomer NMR signal compared to its initial value at $t = 0$. The conversion is defined as $\mathrm{conv}(t) = [1 - [M]_t/[M]_0]$ and finally the amount of formed polymer is given by $\phi_p(t) = \mathrm{conv}(t)\,\phi_0$ and the molecular weight of the growing chain by $M_w(t) = \mathrm{conv}(t)\,M_{w,\infty}$. Here $M_{w,\infty}$ is the molecular weight of the terminated polymer. So by combining reaction kinetics from NMR and SANS results for the final polymer we can finally calculate the expected forward scattering $I(Q=0,t)$ during the in situ experiment as a function of reaction time t. It turns out that once again concentration effects given by the second virial coefficient A_2 play a crucial role. In principle, we also have a time-dependent A_2, but in a zero order approximation, we can assume a constant value for low M_w. Using the values obtained from analysis of the terminated polymer, see above, we can therefore directly calculate the expected time-dependence of the forward scattering intensity.

Table 3. SEC Analysis Results of the Fully Polymerized Samples

	P1		P2		
samples	M_n (kg/mol)	M_w/M_n	M_n (kg/mol)	M_w/M_n	mass fraction of P1
SEC (100 min)	22.3	1.12	124	1.23	87.4
NMR (−10 °C)	27.8	1.11	131	1.67	85.2
NMR (20 °C)	26.2	1.16	140	1.37	86.0
SANS (20 °C)	24.4	1.13	123	1.35	87.5

In Figure 12, we show the calculated total forward scattering intensity $I_{total}(Q=0)$ based on our results we obtained from the "classical" kinetic SEC experiment. In performing this calculation we have to rely on two assumptions: (i) the molecular weight distribution does not substantially change with temperature, since our time-resolved SEC experiment was performed at −8 °C and our in situ SANS experiment was performed at 20 °C. (ii) The molecular weight distribution does not substantially change with time/conversion. The validity of both assumptions is documented in Tables 2 and 3. The agreement with experimental data is striking. In addition, we show the calculated intensity for the individual components.

Finally, the same calculations can now be done to cover the full time and Q-dependence of our SANS data. This calculation are performed in analogy to those for terminated SANS and SEC predictions and are shown in Figure 13. Again a very good agreement between expected and observed scattering SANS data is found. Only in the low Q range we observe some deviations for the early times/low conversion region. This agreement shows that our assumption of nonaggregated chains is valid at all stages of the polymerization.

Conclusions

Our SEC work has shown that the pyridylamidohafnium catalyst contains at least three different polymerization active species. About 98% of the active catalyst shows moderate activity. The polymer resulting from this catalyst fraction shows a relatively narrow molecular weight distribution of $M_w/M_n =$ 1.1 to 1.2. The initiation process of these species is slow, compared to the propagation event. This explains at least partially the broader molecular weight distribution. The second catalyst fraction, which represents about 2% of the catalyst, exhibits an increased activity. Therefore, about 11 wt % of the final polymer are produced by this catalyst. With respect to molecular weight distribution and retarded initiation process, the second catalyst fraction shows behavior similar to the first. It is possible that this second catalyst component consists of several individual structures having slightly different activities. The third catalyst fraction comprises a very small amount of material. It is highly active. Therefore, the molecular weight of the polymer produced with this catalyst is extremely high.

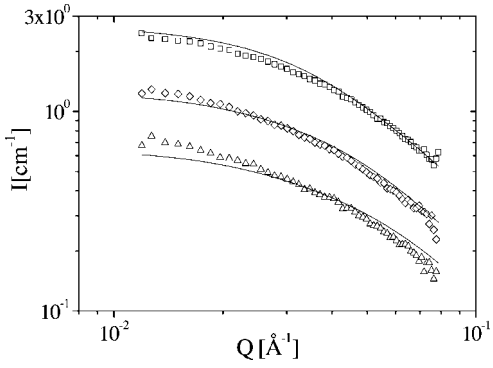

Figure 13. Comparison between calculated time and Q-dependent scattering intensity based on SEC results and SANS data: (Δ) 4 min; (◇) 7 min; (□) 28 min.

Because of the broad molecular weight distribution it ranges from about 5×10^5 to more than 10^7. The mass fraction of polymer resulting from this catalyst is only about 1%. It is thus very difficult to measure by conventional RI detection. However, light scattering detection, which is much more sensitive in the high molecular weight region, clearly reveals this material. Its average molecular weight is on the order of 2.5×10^6. Hence the catalyst fraction responsible for the growth of the very long chains is present in about 100 ppm. Although the overall material contains only a very small fraction of very high molecular weight polymer, it can massively influence material properties, for example in processing.

One possible explanation for the highly active polymerization species giving rise to the higher molecular weight poly(1-octene) is that the catalyst contains a minor, hyper-active fraction. The ligand for the catalyst precursor is prepared from 2,6-diisopropylaniline. The commercial grades of this starting material are typically of a purity no higher than 97%; the major impurities being 2-isopropyl-6-*n*-propylaniline and 2,4-diisopropylaniline. We attempted to purify the aniline by several recrystallizations of the hydrochloride salt from hot isopropanol. This increased the purity as measured by GC analysis to ca. 99%. However, it is possible that a small amount of ligand bearing the less sterically demanding 2,4-diisopropylaniline moiety was retained in the catalyst precursor synthesis and that the catalyst is contaminated with a trace of the 2,4-diisopropylphenyl-bearing hafnium complex, which due to its more open coordination site, would be expected to be a more active olefin polymerization catalyst. Studies to clarify this hypothesis are currently underway.

SANS is an ideal tool to investigate possible aggregation processes of the ionic head groups taking place during the polymerization event. In such a study it is necessary to compare the expected scattering profile of nonaggregating chains with the real SANS data of the growing chains. This requires the knowledge of polymer chain concentration and molecular weight as a function of time. This information can be extracted from in situ NMR data, by comparing signal intensities of the growing polymer and the initiating unit. Additionally, a living process is required: In other words the number of growing chains is constant and no termination processes occur. In our present work two major polymerization processes with different rate constants take place simultaneously and the initiating units cannot be detected in NMR. Therefore time-resolved SEC was used as an additional method to measure molecular weights and relative amounts of each polymer fraction.

In this scenario, it is essential that the polymerization samples used for the different methods agree in their composition. Table 3 summarizes molecular weights, molecular weight distributions and the mass fractions of the main component P1, extracted from SEC measurements of the final samples. The results show good agreement of the different samples within the expected error of SEC measurements of 5−10%.

If the NMR and SEC results are used as an input for the SANS study there is a good agreement between expected scattering profile for nonaggregated chains and measured profiles. At all stages during the polymerization process isolated growing polymer chains were detected. Additionally, our work shows that less than perfectly living systems are useful for structural in situ studies. Also more complex polymerization processes, leading to more complex product mixtures, can be analyzed quantitatively. In the case of the 1-octene polymerization, we examined in this work, most of the monomer is converted into the main polymer product, having a relatively narrow molecular weight distribution. The overall mass fraction of higher molecular weight product is only about 11%. However, in terms of scattering intensity the products of higher molecular

weights dominate (see Figure 5), which complicates the SANS analysis. But it should be pointed out that the SANS analysis can be carried out only with the additional information from NMR and SEC about molecular weights and distributions of the single polymerizing species. Such a time-resolved "multi-techniques" approach will certainly help in the search for more efficient catalysts, optimization of reaction conditions and even clarification of reaction kinetics and mechanism in any polymerization process.

Acknowledgment. A.N. gratefully acknowledges financial support from the Deutsche Forschungsgemeinschaft (DFG) under Grant NI 915.

References and Notes

(1) Beck, S.; Geyer, A.; Brintzinger, H.-H. *Chem. Commun.* **1999**, 2477–2478.
(2) Alonso-Moreno, C.; Lancaster, S. J.; Zuccaccia, C.; Macchioni, A.; Bochmann, M. *J. Am. Chem. Soc.* **2007**, *129*, 9282–9283.
(3) Bryliakov, K. P.; Babushkin, D. E.; Talsi, E. P.; Voskoboynikov, A. Z.; Gritzo, H.; Schröder, L.; Damrau, H.-R. H.; Wieser, U.; Schaper, F.; Brintzinger, H.-H. *Organometallics* **2005**, *24*, 894–904.
(4) Song, F.; Lancaster, S. J.; Cannon, R. D.; Schormann, M.; Humphrey, S. M.; Zuccaccia, C.; Macchioni, A.; Bochmann, M. *Organometallics* **2005**, *24*, 1315–1328.
(5) Zuccaccia, C.; Stahl, N. G.; Macchioni, A.; Chen, M.-C.; Roberts, J. A.; Marks, T. J. *J. Am. Chem. Soc.* **2004**, *126*, 1448–1464.
(6) Beck, S.; Lieber, S.; Schaper, F.; Geyer, A.; Brintzinger, H.-H. *J. Am. Chem. Soc.* **2001**, *123*, 1483–1489.
(7) Stahl, N. G.; Zuccaccia, C.; Jensen, T. R.; Marks, T. J. *J. Am. Chem. Soc.* **2003**, *125*, 5256–5257.
(8) Macchioni, A. *Chem. Rev.* **2005**, *105*, 2039–2073.
(9) Zuccaccia, D.; Bellachioma, G.; Cardaci, G.; Ciancaleoni, G.; Zuccaccia, C.; Clot, E.; Macchioni, A. *Organometallics* **2007**, *26*, 3930–3946.
(10) Babushkin, D. E.; Brintzinger, H.-H. *J. Am. Chem. Soc.* **2002**, *124*, 12869–12873.
(11) Li, H. B.; Marks, T. J. *Proc. Natl. Acad. Sci. U.S.A.* **2006**, *103*, 15295–15302.
(12) Salata, M. R.; Marks, T. J. *J. Am. Chem. Soc.* **2008**, *130*, 12–13.
(13) Niu, A. Z.; Stellbrink, J.; Allgaier, J.; Willner, L.; Richter, D.; Koenig, B. W.; Gondorf, M.; Willbold, S.; Fetters, L. J.; May, R. P. *Macromol. Symp.* **2004**, *215*, 1–15.
(14) Niu, A. Z.; Stellbrink, J.; Allgaier, J.; Willner, L.; Richter, D.; Koenig, B. W.; Gondorf, M.; Willbold, S.; Fetters, L. J. *Physica B* **2004**, *350*, e921–e925.
(15) Niu, A. Z.; Stellbrink, J.; Allgaier, J.; Willner, L.; Radulescu, A.; Richter, D.; Koenig, B. W.; May, R. P.; Fetters, L. J. *J. Chem. Phys.* **2005**, *122*, Art. No. 134906.
(16) Domski, G. J.; Lobkovsky, E. B.; Coates, G. W. *Macromolecules* **2007**, *40*, 3510–3513.
(17) Boussie, T. R.; Diamond, G. M.; Goh, C.; Hall, K. A.; LaPointe, A. M.; Leclerc, M. K.; Murphy, V.; Shoemaker, J. A. W.; Turner, H.; Rosen, R. K.; Stevens, J. C.; Alfano, F.; Busico, V.; Cipullo, R.; Talarico, G. *Angew. Chem., Int. Ed.* **2006**, *45*, 3278–3283.
(18) Boussie, T. R.; Diamond, G. M.; Goh, C.; Hall, K. A.; LaPointe, A. M.; Leclerc, M. K.; Lund, C.; Murphy, V. Symyx Technologies, Inc. PCT Int. Appl. WO 038628, 2002.
(19) Arriola, D. J.; Carnahan, E. M.; Hustad, P. D.; Kuhlman, R. L.; Wenzel, T. T. *Science* **2006**, *312*, 714–719.
(20) Higgings, J.; Benoit, H. In *Polymers and Neutron Scattering*; Oxford University Press: Oxford, 1994.
(21) Chen, E. Y. X.; Marks, T. J. *Chem. Rev.* **2000**, *100*, 1391–1434.
(22) Beaucage, G. J. *J. Appl. Christallogr.* **1995**, *28*, 717–728.
(23) Brant, P.; Ruff, C. J.; Sun, T. *Macromolecules* **2005**, *38*, 7181–7183.

MA8020294